ChemPubSoc Europe

DOI: 10.1002/ejic.201501206

European Journal of Inorganic Chemistry

Full Paper

Characterizing Radicals

Bipyridinium-bis(carboxylate) Radical Based Materials: X-ray, EPR and Paramagnetic Solid-State NMR Investigations

Oksana Toma,[a] Maxime Leroux,[a] Nicolas Mercier,*[a] Magali Allain,[a] Abdel Hadi Kassiba,[b] Shashi Kumar Kumara Swamy,[b,c] and Jens Dittmer*[b]

Abstract: The zwitterionic 1,1′-bis(4-carboxyphenyl)-4,4′-bipyridinium (bp4pc) has been synthesized and crystals of its hydrated form bp4pc·2H_2O and of its protonated reduced form H-bp4pc have been obtained. Upon heating, bp4pc·2H_2O undergoes partial dehydration, leading to bp4pc·H_2O at 160 °C, together with a color change from yellow (room temperature) to green (140 °C) and finally to brown (160–180 °C). Analysis of bond lengths in the solid state reveals the expected short (d = 1.425 Å) and long (d = 1.485 Å) C–C central bond lengths in the all-radical salt H-bp4pc and bp4pc·2H_2O, respectively, whereas the distance of 1.475 Å in bp4pc·H_2O does not allow a conclusion to be drawn regarding the presence of radicals in this compound. EPR and solid-state paramagnetic NMR experiments of H-bp4pc and the hydrated zwitterion bp4pc·2H_2O at different temperatures, however, show that the color change of the latter upon heating is due to the presence of bipyridinium radicals, the concentration of which, although low, increases with increasing temperature. The nature of the electron donor involved in this thermal-induced electron transfer is not fully understood. Most plausible is the possibility that it is the carboxylate group with an intramolecular electron-transfer process; on the other hand it, cannot be excluded that the electron stems from the water molecule, which decomposes into O_2, H^+, and e^- giving H-bp4pc entities.

Introduction

1,1′-Disubstituted 4,4′-bipyridinium dications [also called viologens (V^{2+}), with the most famous being the 1,1′-dimethyl-4,4′-bipyridinium or methylviologen] are a well-known class of redox couples that undergo two reversible, one-electron reductions to a radical cation and the neutral form. Viologens have afforded a great number of charge-transfer (CT) complexes and salts, but the main applications in chemistry of viologens take advantage of the first reversible reduction step involving the two stable V^{2+} and $V^{\cdot+}$ forms; in particular because of the color change during the redox process, which can occur either in solution or in the solid state because of the different absorption domains of V^{2+} (UV) and $V^{\cdot+}$ (visible).[1] The chemistry of $V^{\cdot+}$ radical cations in solution has been well documented, but to a much less extent in the solid state. Notably, crystal structures based on viologen radicals are rare.[2] Whereas the reduction process from V^{2+} to $V^{\cdot+}$ can be achieved either electrochemically or chemically, viologen radical cations can also be generated photochemically as a result of an electron transfer from an electron donor towards bipyridinium cycles.[3] This has led to the development of several families of photochromic materials based on viologens, including zeolite compounds,[4] polycyanopolycadmates chlatrates,[5] halometalate hybrids,[6] and coordination polymers (CP) with carboxylate ligands.[7–10] If the photochromic phenomenon is not completely elucidated; however, it was shown that suitable donor-acceptor intermolecular interactions are necessary to observe the photoinduced electron transfer. On the one hand, good electron donors will lead to direct charge-transfer processes whereas worse electron donors can potentially lead to PICT processes.[1] On the other hand, short contacts between N^+(pyridinium) centers and electron donors (X atoms or molecules) must occur.[3] In addition, it was shown that the process is efficient because the (N^+···X) direction is perpendicular to the pyridinium ring, as exemplified in a series of halometalate hybrids.[6] Other examples can be taken from the growing field of photoactive CP, including carboxylate ligands based on pyridinium or bipyridinium units. For instance, 1,1′-bis(4-carboxybenzyl)-4,4′-bipyridinium in the presence of 1,4-benzenedicarboxylate (BDC^{2-}) and Cd^{2+} afforded a photochromic interpenetrated network CP in which a sandwich-type stacking D···A···D (A = viologen, D = BDC^{2-}) is formed, the photochromic properties being related to the position of one carboxylate O atom, which is approximately perpendicular to the pyridinium ring at the N atom, with an O···N^+ distance of 3.57 Å.[7] In another interesting CP compound, the release of water guest molecules modifies the characteristics of the N^+(pyridinium)···O(carboxylate) contacts, and whereas the dehydrated phase is photochromic due to specific N^+···O interac-

[a] MOLTECH ANJOU, UMR-CNRS 6200, Université d'Angers,
2 Bd Lavoisier, 49045 Angers, France
E-mail: nicolas.mercier@univ-angers.fr
http://moltech-anjou.univ-angers.fr/Site/equipe_cimi.htm
[b] Institut des Molécules et des Matériaux du Mans, CNRS UMR 6283,
Université du Maine,
Avenue Olivier Messiaen, 72085 Le Mans cedex , France
E-mail: jens.dittmer@univ-lemans.fr
[c] Institut de Chimie de la Matière Condensée de Bordeaux, CNRS-UPR 9048,
87 Avenue du Docteur Schweitzer, 33608 Pessac cedex, France

Supporting information for this article is available on the WWW under http://dx.doi.org/10.1002/ejic.201501206.

tions, the hydrated phase is not.[8a] In these CP compounds, the carboxylate group interacting with pyridinium cycles belongs either to neighboring pyridinium-carboxylate ligands[7,9] or to independent carboxylate ligands such as BDC^{2-}.[8]

The properties of neutral zwitterionic viologen have been much less exploited.[11–13] Whereas the first photochromic zwitterionic viologen was based on sulfonate groups,[12] a recent report concerns a viologen bearing carboxylate groups.[13] As in CP compounds, similar structural features are observed with short $N^+\cdots O$ (sulfonate or carboxylate) contacts and suitable angles between the pyridinium cycle and the ($N^+\cdots O$) direction. The presence of viologen radicals in all such compounds is typically characterized by EPR spectroscopic analysis. Solid-state NMR spectroscopy is a standard technique for the identification of chemical groups and changes of the local order; however, the signals are shifted and broadened in an extreme way by the presence of unpaired electrons. On the other hand, there has been substantial progress over the last years in dealing with this perturbation, particularly with very fast magic-angle spinning (MAS).[14] Moreover, for several cases of organic compounds complexing paramagnetic metal ions, it was shown that one can exploit the hyperfine interaction in terms of better hydrogen resolution because of the signal dispersion, correlation of the hyperfine shift to the structure by means of DFT calculations,[15] and the measurement of distances by electron-nuclear relaxation experiments.[16] Radicals are used in NMR analysis of solutions, which is commonly more advanced, as tags to give additional constraints for the structure determination of biomolecules, and for signal enhancement by dynamic nuclear polarization (DNP). For solids, however, there are hitherto only a few NMR studies of organic radicals published.[17]

In this article, we describe the synthesis of the zwitterionic 1,1′-bis(phenyl-4-carboxylate)-4,4′-bipyridinium (bp4pc), the preparation of crystals of its hydrated form bp4pc·$2H_2O$ and its protonated reduced form H-bp4pc, as well as crystal structures, EPR and paramagnetic solid-state NMR characterization. We will show that partial dehydration of bp4pc·$2H_2O$ to bp4pc·H_2O (160 °C), which is accompanied by a color change from yellow (room temperature) to brown (160–180 °C) involves the formation of bipyridinium radicals, as first revealed by EPR measurements. Moreover, ^1H and ^{13}C NMR spectra, assigned with the help of DFT calculations and correlation spectra, show that the nature of the thermoinduced radicalic units in bp4pc·H_2O correspond well to the $bp4pc^{\bullet-}$ radicalic entities found in the all-radical compound H-bp4pc. The origin of this thermoinduced electron-transfer will be discussed.

Results and Discussion

Thermal Behavior and EPR Characterization

Crystals of bp4pc·$2H_2O$ were grown under hydrothermal conditions at 100 °C. They are obtained mainly as needle-like yellow crystals. The TGA curve of the powder sample of bp4pc·$2H_2O$ shows a first weight loss in the 100–160 °C range following by decomposition starting at 300 °C (see the Supporting Information, Figure S3). The first feature is attributed to a complete dehydration, with the weight loss corresponding to $2.2H_2O$ per formulation unit. The water release is slower in the case of a sample consisting of crystals. Thus, the TGA curve of crystals of bp4pc·$2H_2O$ previously heated at 160 °C for more than one hour shows a first weight loss of 5 % corresponding to the loss of approximately one molecule of water per formulation unit, indicating that the heated crystals have a formulation of bp4pc·H_2O, in good accordance with the result of the crystal structure analysis. Interestingly, the dehydration involves a color change of crystals, as can be seen in the images in Figure 1 for viologen (V^{2+}) based compounds. A dark-blue to black color of samples usually indicates the presence of $V^{\bullet+}$ radicals, which are known to absorb in the visible range because of a SOMO to LUMO transition.[1] For instance, crystals of H-bp4pc are black, in good accordance with the expected presence of $bp4pc^{\bullet-}$ radicals besides the H^+ entities in the corresponding structure (see below). Finally, the development of yellow to brown color upon dehydration of bp4pc·$2H_2O$ could indicate the presence of bipyridinium radical cations as a result of a thermoinduced electron-transfer from an electron-donor unit to the bipyridinium electron-acceptor units.[1,3] To characterize organic radicals in these compounds, EPR measurements were carried out on crystalline samples. The features of the EPR signals are depicted in Figure 2. For the crystalline H-bp4pc sample, the EPR spectrum was recorded at room temperature (Figure 2, a), whereas the EPR signal for the bp4pc·$2H_2O$ sample was recorded at different temperatures in the range form room temperature to 190 °C. Compound bp4pc·$2H_2O$ exhibits a very weak EPR signal with broad features at room temperature, indicating very small residual unpaired spin concentration, whereas the signal becomes higher and sharper from 140 to 190 °C (Figure 2, b and c). The EPR signal of the all-radicalic compound H-bp4pc is approximately 400 times higher than that of bp4pc·$2H_2O$ heated to 190 °C (measurements on a same quantity of sample). This means that the radical concentration in the partially desolvated compound remains very weak (less than 0.5 % of the bp4pc units). In the bp4pc·$2H_2O$ sample, the development of the unpaired spin concentration is accompanied by a drastic decrease of the line width. This can be explained by the mobility of the thermally delocalized electrons over the material backbone and leads to what is termed motional narrowing of the EPR line width. This conclusion is also supported by the decrease with temperature of the average g-factor, which characterizes the electronic state of the paramagnetic species (as unpaired electrons) (see the Supporting Information, Figure S4). As the delocalization is established, the unpaired spins interact weakly with their environments. The change in the value of the *g*-factor from that of a free electron (2.0023) is generally induced by

Figure 1. Photos of a single crystal of bp4pc·$2H_2O$ at room temperature (left), heated at 140 °C (middle), and heated at 160 °C (right).

spin-orbit coupling between the electron spin and the orbital wave function for the location of the unpaired electrons on defined atoms of the materials. As the mobility increases, the residence probabilities of electrons in the vicinity of defined atoms are too low to contribute to the spin-orbit coupling terms. This change in the EPR signal is irreversible when returning to room temperature.

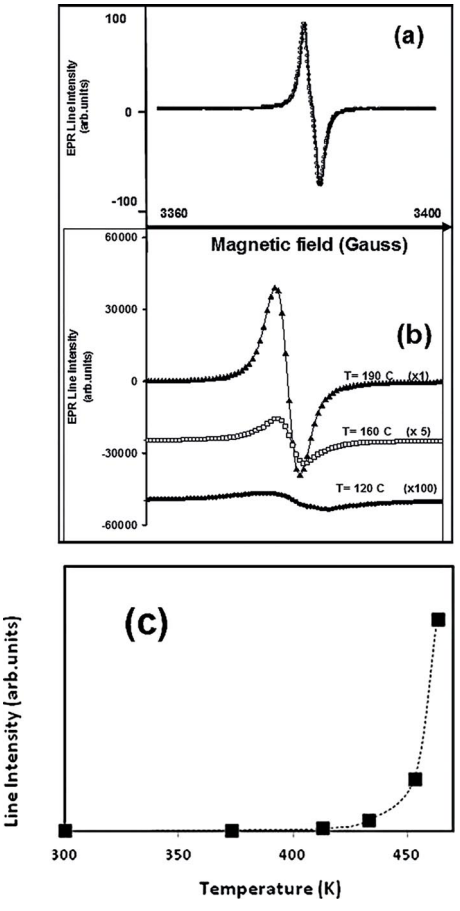

Figure 2. (a) EPR spectrum of a crystalline H-bp4pc sample recorded at room temperature. (b) EPR spectra of bp4pc·2H_2O at 120 °C (full squares), 160 °C (empty squares) and 190 °C (black triangles), scaled by a factor of 100, 5, and 1, respectively, and (c) EPR line intensity vs. heating temperature.

X-ray Structures

The crystal structure of H-bp4pc has been solved in the $P2_1/n$ space group. The asymmetric unit contains half a bp4pc unit and one H atom located on a symmetry center. As a result, there is one H^+ cation per bp4pc unit, meaning that each of the molecular units bear a negative charge of –1. This can be explained by a reduction of the bipyridinium dicationic core to a radical cationic part during the synthesis, finally leading to the bp4pc$^{\bullet-}$ radical anionic entities. The presence of organic radicals, which was confirmed by EPR and NMR experiments (see below), was first indicated by analysis of the intramolecular bond lengths. Particularly, the central C–C bond of 1.427(2) Å is typical of bipyridinium radicals,[2] and corresponds to a intermediate bond length between a single C–C bond length ($d \approx$ 1.48 Å) of dicationic viologen units and a double C=C bond length in the quinoid-type structure of a di-reduced neutral form of viologens ($d \approx$ 1.36 Å).[1] The bp4pc$^{\bullet-}$ molecular units are linked together through shared H atoms [d(O1–H1) = 1.229(1) Å], leading to infinite supramolecular chains along the (a–c) direction (Figure 3, b). In the (a, c) plane, molecules of adjacent chains also interact through N$^+$···O2(carboxylate) contacts [d = 3.345(2) Å].

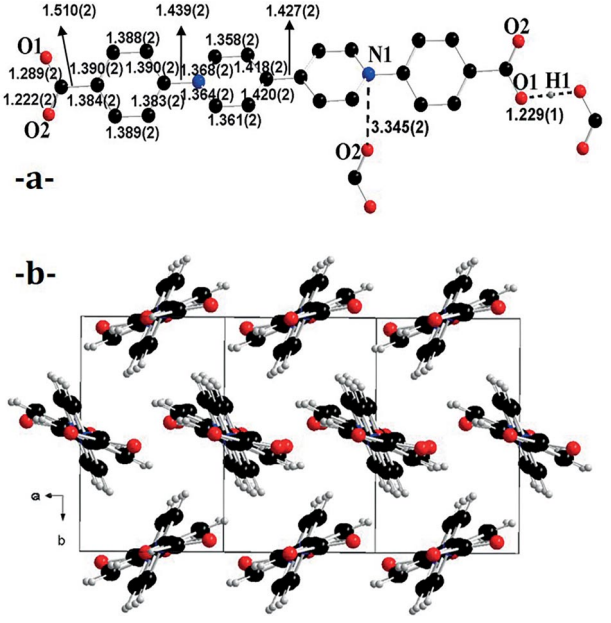

Figure 3. Crystal structure of H-bp4pc: partial view showing intermolecular interactions and intra- and intermolecular bond lengths (H atoms, except the H1 shared atom, omitted for clarity) (a), and a general view along the chain axis (b).

The crystal structure of bp4pc·2H_2O has been solved in the $C2/c$ space group. The asymmetric unit contains one water molecule and half a bp4pc molecule. The general layout of the structure can be described as slabs of bp4pc molecules, which are roughly parallel to the plane defined by the b direction and the (a + c/2) direction (Figure 4, a). One slab is displayed in Figure 4 (b). It shows the hydrogen bonds between the two H atoms of water molecules and carboxylate parts of two adjacent molecules, finally leading to a zig-zag 1D hydrogen-bonding network. The electron-rich part of water molecules interacts with N atoms of the pyridinium cycles of bp4pc belonging to adjacent slabs. An impressively short N$^+$···OH_2 distance of 3.012(2) Å is observed, which is much smaller than N$^+$···O$^-$(carboxylate) contacts reported in other carboxylate based materials.[7–9] In addition, the angle between the pyridinium ring and the (N$^+$···O) direction (80.3°) is close to 90°, which is a key indicator for the observation of photochromic properties in related materials.[3] Together, these results indicate a strong donor/acceptor interaction. Nevertheless, despite favorable structural features, the material is not photochromic, which is certainly due to the nature of the donor entity: to our knowledge, no photoinduced electron transfer from water molecules to bipyridinium parts has been reported.

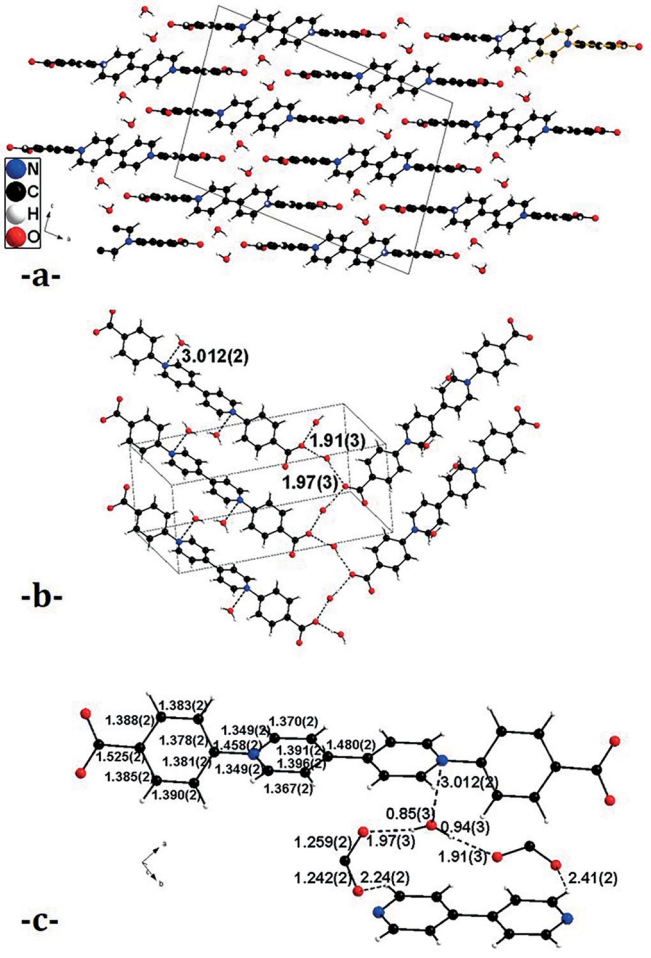

Figure 4. Crystal structure of bp4pc•2H_2O at room temperature: general view (a), view of one slab showing the 1D hydrogen network defined by carboxylate groups and water molecules, and short N^+···OH_2 contacts (b), and partial view showing intermolecular interactions and intra- and intermolecular bond lengths (c).

As the loss of water molecules involved a color change due to the appearance of bipyridinium radical cations, X-ray analysis of the partially desolvated crystal was of interest, particularly because the bond lengths in viologen radicals, as in the case of H-bp4pc, are changed compared with those encountered in viologen dications. Figure 4 (c) gives details of the intramolecular bond lengths of the room-temperature crystal structure of bp4pc•2H_2O, whereas those of bp4pc•H_2O [crystal of bp4pc•2H_2O previously heated at 160 °C] are given in Figure S1. In both structures, the central C–C bond length is typical of a C–C single bond; that is, 1.480(2) Å in the structure of bp4pc•2H_2O (as expected), and 1.474(2) Å in the structure of bp4pc•H_2O, showing that we cannot deduce the presence of radicals from the structural data of bp4pc•H_2O. At least, this indicates that, if radicals are present, their concentration is very low. This is in agreement with EPR and NMR measurements (see below).

The intermolecular interactions are not very different between both structures either. Nevertheless, we notice a dissymmetrical situation of H_2O···O(carboxylate) contacts between the O atom of water molecules and O atoms of neighboring carboxylate groups: in bp4pc•H_2O, d = 2.754(5) Å and d = 2.826(5) Å (Figure S1), whereas d = 2.811(3) Å and d = 2.794(3) Å in the structure of bp4pc•2H_2O (Figure 4, c). An interesting point concerns the nature of the electron donor in this thermal-induced electron-transfer leading to bipyridinium radical cations. The release of water molecules that were in strong donor–acceptor interactions with bipyridinium cores certainly impacts the electron-acceptor behavior of molecules, and further the electron transfer towards bipyridinium parts. The best candidate as electron donor is certainly the carboxylate group, which is known to act as an electron donor in bipyridinium materials exhibiting photo- or thermochromism.[7–10] However, in contrast to the situation observed in structures of such photo- or thermochromic materials, the oxygen atoms of carboxylate groups do not interact directly with the N sites of pyridinium cycles in the structure of bp4pc•xH_2O (x = 1, 2). Nevertheless, two indirect electron-transfer pathways may be possible: an intramolecular process through the phenyl ring as already proposed by Lv et al.,[6d] or an intermolecular process from an oxygen atom to the pyridinium ring through short lateral O···H contacts [d = 2.21(2) Å, see Figure 4, c] as suggested previously.[18] Another hypothesis concerning the nature of the electron-donating group can also be suggested: could a small quantity of water molecules (less than 1 % according to NMR and EPR analysis) be decomposed into O_2, H^+ and electron, finally acting as a reducing agent leading to the formation of (H^+,bp4pc$^{•-}$) entities as found in the all-radical material H-bp4pc? Finally, we must note that, unlike other such photochromic materials,[7,8a] the electron-transfer process is not reversible by keeping the sample for a long time at room temperature in air or in a high-humidity atmosphere.

Solid-State NMR Spectroscopic Analysis

By using fast magic-angle spinning, ^{13}C and even ^{1}H NMR analysis can identify and characterize organic matter with paramagnetic centers. This has been shown in particular for metal-organic systems.[14–16] Figure 5 compares, among others, the ^{1}H spectrum of bp4pc•2H_2O and H-bp4pc under 60 kHz MAS. Compound bp4pc•2H_2O shows essentially one broad, unresolved signal spanning over the entire classical spectral range of 0–10 ppm, as typical for ^{1}H solid-state NMR spectroscopy. In contrast, H-bp4pc shows several signals that are shifted far beyond this range. This can only be due to the presence of an unpaired electron, the hyperfine coupling to which causes these Fermi-contact shifts. A further understanding of the paramagnetic center can be achieved by correlation to ^{13}C spectra and the comparison with DFT calculations of the shifts of both nuclei. Figure 6 (A) shows a ^{1}H-^{13}C dipolar INEPT correlation spectrum optimized for paramagnetic organic molecules at 40 kHz MAS.[15,16] Note that in Figure 5 the ^{1}H signals are slightly less shifted by the higher sample temperature because of the faster spinning (Curie's law). On top of the ^{13}C axis, a ^{13}C DEPTH direct excitation spectrum with background suppression with very short recycle delay (27 ms in total, exploiting the fast relaxation) for efficient signal accumulation (1024 K repetitions) is shown. The spectrum is consequently not fully quantitative. Most of

the signals are likewise shifted beyond the typical diamagnetic range of 0–220 ppm. To assign the signals to atoms and to validate the model, the spectra are compared to total shifts (sum of chemical and Fermi-contact shifts) determined by calculating the electronic spin densities. These calculations cannot currently be expected to be very accurate, but they usually correctly predict the range in which the signal can be expected.[19] Indeed, the pattern of the calculated ^{1}H signals corresponds quite well to the shifted signals of the experiment. The spin density (the density of the unpaired electron) is represented in Figure 6 (B) in the form of mesh plots with two different minimal contour levels to either focus on the radicalic center or show the influence on the hydrogen by delocalization of the unpaired spin and spin polarization. The strongest spin density lies, as expected, on the nitrogen atoms; however, the neighboring carbon atoms also reach up to 20 % of that of the nitrogen atoms at the nucleus. The hydrogen atoms generally bear a smaller probability of the presence of an unpaired spin, but this is still sufficient for sizeable shifts, in particular those in the pyridinium ring. They lead to the signal structure at –82 and –105 ppm (–85 and –116 ppm in the calculations) for H2/5 and H3/4, respectively. Among the protons of the outer benzene rings, those closer to the nitrogen (H7/11) should resonate at –40 ppm, corresponding to the observed signal at –36 ppm. The outer protons (H8/10) are calculated to have a positive hyperfine shift, as can also be seen from the positive spin density at these hydrogen atoms (Figure 6, B). Correspondingly, there is a signal with positive shift observed at δ = +38 ppm (calcd. +41 ppm). An uncertainty is in H1, assigned to 20 ppm: being far from the radicalic center it is only slightly shifted (calcd. 6.4 ppm); however, the influence of the neighboring molecule is not taken into consideration in the calculations and there are residual diamagnetic signals of non-radical impurities in the same range.

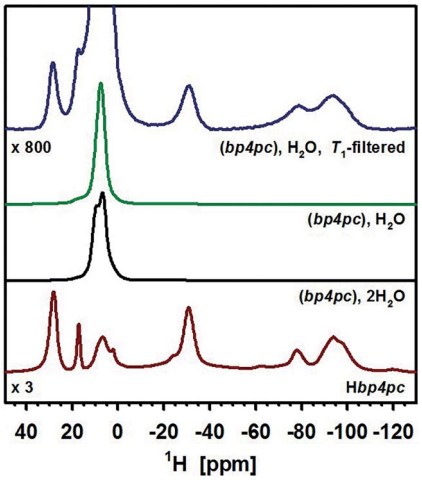

Figure 5. ^{1}H spectra under 60 kHz MAS of H-bp4pc, bp4pc·2H_2O, bp4pc·H_2O, and bp4pc·H_2O with a T_1 filter against diamagnetic signals. Scaling according to the number of repetitions, multiplied by the factor indicated.

Correlations to ^{13}C signals, supporting the previous assignment, are observed between H7/11 and C7/11 at δ = 600 ppm (calcd. 636 ppm) as well as H2/5 and C2/5 at –150 ppm (calcd. –289 ppm). The correlation spectrum allows the overlapping

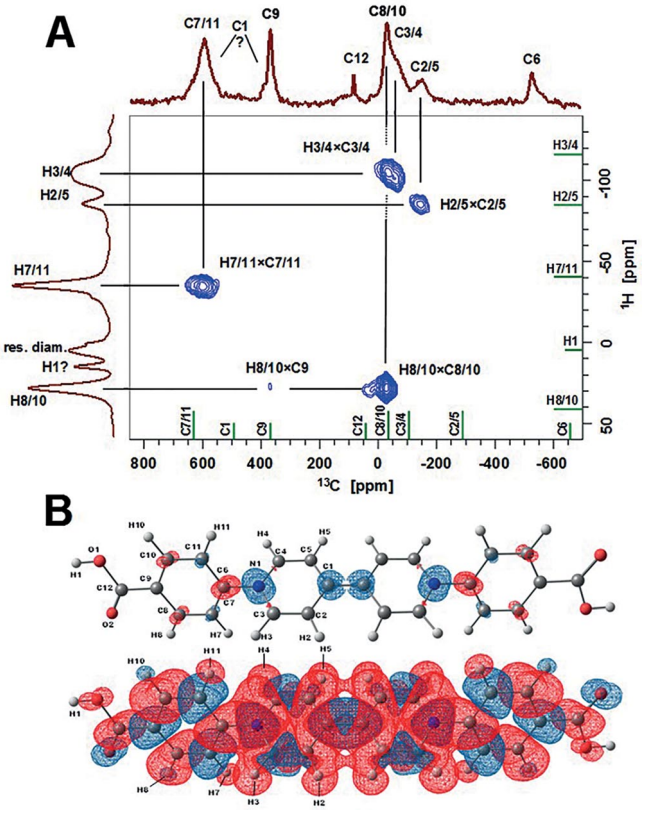

Figure 6. (A) ^{1}H, ^{13}C, and ^{1}H-^{13}C dipolar INEPT correlation spectrum of H-bpc4pc with assignment. MAS 40 kHz. The green bars indicate the signal positions predicted by DFT calculations. (B) Spin density of H-bp4pc calculated by DFT in two different representations. Top: the blue mesh represents a contour surface at $+10^{-3}$ a.u., the red grid at -10^{-3} a.u. Bottom: the surfaces are at $\pm 5 \times 10^{-5}$ a.u.

^{13}C region between 0 and –120 ppm to be separated by cross peaks to H3/4 and H8/10. The signal for C12 (calcd. 47 ppm, exp. 75 ppm) is reduced by the fast repetition technique because it is far from the radicalic center, rendering its longitudinal relaxation for equilibrium recovery less rapid. Residual diamagnetic carbon signals are suppressed by the same effect. Like C12, carbon atoms C6 (exp. –540 ppm, calcd. –663 ppm) as well as C1 do not have cross peaks because there is no proton attached. Carbon C9 (exp. 360, calcd. 367 ppm) however receives a small part of magnetization from H8/10. The assignment of C1 (calcd. 490 ppm) is ambiguous; it seems to overlap either with C7/11 or C9. In general, however, the signal pattern resulting from the DFT calculations is in agreement with the NMR spectra, with a tendency to overestimate in particular the carbon hyperfine shift by an order of 5–10 %. Overall, this confirms the molecular model with radical centers at both nitrogen atoms in resonance. If there was any asymmetry in the molecule (tested by DFT for different models), a double set of signals would be expected.

The ^{1}H spectrum of bp4pc·H_2O (thus after heating to 180 °C) shown in Figure 5 (green line) is diamagnetic and not very different from bp4pc·2H_2O (before heating). Nevertheless, there is a color change, and EPR spectroscopic analysis (Figure 2) shows the presence of paramagnetic centers in low concentration. We

apply a T_1 filter against the dominating diamagnetic signals by a very short recycle delay (7 ms including the acquisition time), the DEPTH sequence against baseline artifacts and subtract the empty rotor signal against residual probe and rotor signals. With this procedure, small hyperfine shifted ^{1}H signals become visible (Figure 5, blue line), but only for bp4pc•H_2O. The spectrum is essentially identical to that of H-bp4pc, suggesting that heating has created a minor contribution of bp4pc$^{\bullet-}$. Under the same experimental conditions, the signals are 220 times smaller than for the H-bp4pc sample, which is in good agreement with the EPR results, leading to the conclusion that the content of this minor species is thus only approximately 0.5 %. With this low percentage, no hyperfine shifted carbon signals can be observed with any technique; however, the carbon spectra of the diamagnetic region, obtained by a CP experiment, give some information about the sample (Figure 7, aromatic region). Whereas bp4pc•$2H_2O$ shows well-defined signals in the sp^2 range between δ = 120 and 150 ppm and the signal from the carboxy group at δ = 169 ppm with line widths of about 200 Hz, after heating they are broadened to a considerable loss of resolution. This shows that bp4pc•H_2O, despite a still well-defined X-ray diffraction pattern, exhibits a substantial structural heterogeneity. Heating has not only led to the removal of – in the majority – one water molecule per bipyridinium unit, but also led to a partial degradation of the sample.

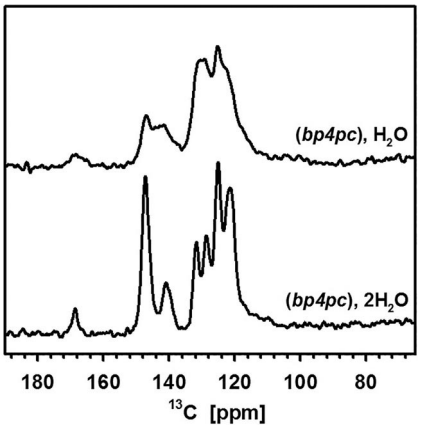

Figure 7. Excerpt of ^{13}C CP spectra of bp4pc•$2H_2O$ as prepared (bottom) and after heating to 180 °C and annealing [bp4pc•H_2O] (top).

Conclusions

In this work, a *bipyridinium-carboxylate* zwitterionic unit bp4pc has been obtained for the first time in its protonated reduced form H-bp4pc (= bp4pc + H^+ + e^-). This all-radical based material has been fully characterized by X-ray diffraction, EPR, and by solid-state NMR analysis, which is a technique that is rarely used for such organic radical materials. DFT calculations of the electronic spin density allow assignment of the NMR signals, and the agreement between calculations and spectra confirms the model of the radical. We also report the hydrated phase of the compound, bp4pc•$2H_2O$, which, upon heating, (i) becomes the partial dehydrated compound bp4pc•H_2O, and (ii) undergoes a change of color. We show that the color is due to the presence of a small quantity of bp4pc$^{\bullet-}$ radicals. Interestingly, the electron-transfer process to the pyridinium rings cannot result, as observed in (nearly) all structures of such photo- or thermochromic materials (bipyridinium and carboxylate units), from the electron-donor O atoms of carboxylate groups to the N^+ sites through short and suitable N^+•••O(CO_2^-) contacts. Two main hypotheses can be proposed: either the electron donor is a carboxylate group, and the electron transfer is an intramolecular process through the phenyl ring, or the electron donor is a water molecule that decomposes into O_2, H^+ and e^- leading to the H^+,bp4pc$^{\bullet-}$ unit as found in the structure of H-bp4pc. Finally, we note that the preparation of H-bp4pc can be very useful in the synthesis of interesting all-radicalic porous coordination polymers. Efforts will be made in this direction and the results will be reported in due course.

Experimental Section

Synthesis and Characterization: The zwitterionic compound bp4pc•$2H_2O$ was prepared by the solvothermal method using a Teflon®-lined PARR autoclave (internal volume 25 mL), from 100 mg of 1,1′-bis(2,4-carboxyphenyl)-4,4′-bipyridinium dichloride (H_2bp4pc)Cl_2[20] in DMF (4 mL), EtOH (2 mL) and H_2O (1 mL). The reaction mixture was heated in a programmable oven with the following parameters: 10 h heating from 25 to 100 °C, 35 h remaining at 100 °C, then 17 h cooling to 25 °C (yield of 60 %). Large yellow needles were collected by filtration and washed with ethanol. H-bp4pc has been obtained fortuitously by exploring the system $ZrOCl_2$, (H_2bp4pc)Cl_2 and fumaric acid in a DMF/HCO_2H (5:1) solution. The heating of the mixture in 6:1:6 ratio at 110 °C in a sealed glass tube led first to the formation of a green solution, typical of the presence of bipyridinium radicals, then to the formation of a small amount of black crystals after a few days. After cooling to room temp. a few milligrams of crystals of H-bp4pc were collected by filtration. Elemental analysis calcd. for bp4pc•$2H_2O$: C 66.66, H 4.66, N 6.48, O 22.20, found: C 66.53, H 4.82, N 6.37, O 22.64; elemental analysis calcd. for H-bp4pc: C 72.50, H 4.31, N 7.04, O 16.10, found: C 72.21, H 4.16, N 7.21, O 15.84.

The powder X-ray diffraction (PXRD) patterns of bp4pc•$2H_2O$ were obtained with a D8 Bruker diffractometer (Cu-$K_{\alpha1,2}$ radiation) equipped with a linear Vantec super speed detector; all the observed reflections could be indexed in the unit cell parameters obtained from single-crystal X-ray diffraction experiments (see the Supporting Information, Figure S2). Differential scanning calorimetry (DSC) and thermogravimetric analysis (TGA) were performed with DSC-2010 and TGA-2050 TA Instruments systems in the range of 20–300 °C and 20–1000 °C, respectively.

X-ray Crystallography: X-ray diffraction data were collected with an Agilent Supernova with Cu-K_α radiation (λ = 1.5407 Å) for H-bp4pc and a Bruker-Nonius KAPPA-CDD with Mo-K_α radiation (λ = 0.71073 Å) for the hydrated phases of bp4pc. Data were first collected at room temperature from a selected single crystal of bp4pc•$2H_2O$. The single crystal was then slowly heated to 160 °C and, after cooling, a second data collection was performed at room temp. All experiments were carried out under a nitrogen atmosphere. A summary of crystallographic data and refinement results for H-bp4pc, bp4pc•$2H_2O$ and bp4pc•$0.8H_2O$ compounds is listed in Table 1. The structures were solved by direct methods and refined on F^2 by full-matrix least-squares method with anisotropic approximation for all non-hydrogen atoms, using the package SHELX97. All

hydrogen atoms were found by Fourier difference map and absorption was corrected by using the program SADABS. For structures of hydrated phases, the site occupancy factor of the oxygen atom of the water molecule was first refined, leading to 0.96 and 0.39 and then fixed to 1 and 0.40 H_2O molecules per asymmetric unit for bp4pc·2H_2O and bp4pc·0.8H_2O, respectively. These values are in good agreement with those found from TGA measurements; that is, 2 and 1 H_2O molecules. In the following, these compounds will be named bp4pc·2H_2O and bp4pc·H_2O. A complete list of crystallographic data, along with the atomic coordinates, the anisotropic displacement parameters and bond lengths and angles for each compound, are given as CIF files.

Table 1. Crystallographic data for H-bp4pc and bp4pc·xH_2O (x = 2, 0.8).

	H-bp4pc	bp4pc·2H_2O	bp4pc·0.8H_2O
Crystal system	monoclinic	monoclinic	monoclinic
Space group	$P2_1/n$	$C2/c$	$C2/c$
a [Å]	7.9053(3)	19.337(2)	19.103(6)
b [Å]	8.0834(3)	7.6059(7)	7.637(2)
c [Å]	14.1427(5)	13.504(1)	13.350(5)
A [°]	90	90	90
B [°]	95.44(1)	97.992(9)	99.73(3)
Γ [°]	90	90	90
Volume [Å^3]	899.67(6)	1966.8(3)	1919.6(11)
Temperature [K]	293	293	293
Refl. collected/ unique	3473/1752	18826/2245	17468/2180
Obsd. reflections [$I > 2\sigma(I)$] [R_{int}]	1491 [0.018]	1412 [0.053]	1262 [0.066]
Parameters	137	185	185
$R_1[I > 2\sigma(I)]/wR_2$ (all data)	0.0421/ 0.1468	0.0456/ 0.1163	0.0530/ 0.1182

CCDC 1415258 (for bp4pc·2H_2O), 1415259 (for bp4pc·H_2O), and 1415260 (for H-bp4pc) contain the supplementary crystallographic data for this paper. These data can be obtained free of charge from The Cambridge Crystallographic Data Centre.

EPR Spectroscopy: EPR experiments were carried out with a Bruker EMX EPR spectrometer working in X-band (9.45 GHz). The modulation field and working power were adjusted to avoid any signal distortion. The samples as powder (ca. 10 mg) of micron-sized crystallites were placed in an ultrapure quartz Suprasil tube and fitted inside the resonant cavity equipped with a quartz Dewar for high-temperature measurements using a Bruker (ER 1114 VT) temperature regulator. For bp4pc·2H_2O, EPR spectra were recorded at different temperatures from r.t. to 190 °C with the aim to characterize the activated unpaired spins upon increasing temperature.

NMR Spectroscopy: NMR experiments were performed with a Bruker Avance III 300 MHz WB spectrometer equipped for samples in the solid phase. Spectra were recorded with a 1.3 mm two-channel probe-head under magic-angle spinning (MAS) with a rate of 40 kHz (^{13}C) or 60 kHz (^{1}H). ^{1}H-^{13}C cross-polarization spectra of the hydrated phase of bp4pc with 1 ms contact time were accumulated over 8 K repetitions with 3 s relaxation delay. ^{13}C spectra of H-bp4pc were acquired with the DEPTH experiment with 1024 K repetitions and 27 ms total recycle delay (time between last and first pulse of the sequence). A 2D ^{1}H-^{13}C dipolar INEPT spectrum was acquired by using the States-TPPI scheme with 64/2 increments to a $t_{1,max}$ of 400 µs. 16 K scans were accumulated with a total recycle delay of 14 ms. ^{1}H spectra were acquired with a relaxation delay of 2 s, or, as T_1 filter, 7 ms. The number of repetitions was 128 (hydrated phase), 256 (H-bp4pc), or 128 K [T_1 filtered bp4pc·H_2O]. To acquire the ^{1}H signals of a paramagnetic minor species of bp4pc·H_2O, 128 K scans were accumulated. The latter experiment was done as DEPTH rather than single pulse. For all ^{1}H experiments, the background signal of an empty rotor was subtracted.

DFT Calculations: Theoretical Fermi contact couplings and the resulting NMR shifts were calculated by means of DFT for the interpretation of the ^{1}H NMR spectra. Basing on the structural models obtained by X-ray diffraction, several models were tested. All calculations were performed by means of the program Gaussian09[21] in the unrestricted (open shell) model using Bethe-style 3 parameter and Lee–Yang–Parr correlation functional (B3LYP). The basis set was 6-311G.

Supporting Information (see footnote on the first page of this article): Synthetic procedures, single-crystal data, PXRD pattern, TGA, EPR. Single-crystal crystallographic data in CIF format.

Acknowledgments

S. K. K. S. and J. D. acknowledge the Region Pays de la Loire for financial support (convention number 2007-11860), O. T. and N. M. are grateful to LUMOMAT (project BipyLum) for funding and M. L. thanks the Université d'Angers for a PhD grant.

Keywords: Solid-state structures · Thermochromism · Viologen · Radicals · NMR spectroscopy

[1] P. M. S. Monk, *The Viologens: Physicochemical Properties, Synthesis and Application of the Salt of 4,4'-Bipyridine*, Wiley, New York, **1998**.
[2] a) B. Emmert, G. Junk, H. Haffner, *Ber. Dtsch. Chem. Ges.* **1924**, *57*, 1792–1797; b) T. M. Bockman, J. K. Kochi, *J. Org. Chem.* **1990**, *55*, 4127–4135; c) W. W. Porter III, T. P. Vaid, *J. Org. Chem.* **2005**, *70*, 5028–5035; d) A. C. Fahrenbach, J. C. Barnes, D. A. Lanfranchi, H. Li, A. Coskun, J. J. Gassensmith, Z. Liu, D. Benitez, A. Trabolsi, W. A. Goddard III, M. Elhabiri, J. F. Stoddart, *J. Am. Chem. Soc.* **2012**, *134*, 3061–3072; e) N. Leblanc, N. Mercier, O. Toma, A. H. Kassiba, L. Zorina, P. Auban-Senzier, C. Pasquier, *Chem. Commun.* **2013**, *49*, 10272–10274.
[3] a) M.-S. Wang, G. Xu, Z.-J. Zhang, G.-C. Guo, *Chem. Commun.* **2010**, *46*, 361–376; b) N. Mercier, *Eur. J. Inorg. Chem.* **2013**, 19–31.
[4] a) Y. S. Park, S. Y. Um, K. B. Yoon, *J. Am. Chem. Soc.* **1999**, *121*, 3193–3200; b) E. L. Clennan, *Coord. Chem. Rev.* **2004**, *248*, 477–492.
[5] a) S. Nishikiori, H. Yoshikawa, Y. Sano, T. Iwamoto, *Acc. Chem. Res.* **2005**, *38*, 227–234; b) H. Yoshikawa, S. Nishikiori, T. Watanabe, T. Ishida, G. Watanabe, M. Murakami, K. Suwinska, T. Luboradzki, J. J. Lipkowski, *J. Chem. Soc., Dalton Trans.* **2002**, 1907–1917.
[6] a) G. Xu, G.-C. Guo, M. Wang, Z. Zhang, W. Chen, J. Huang, *Angew. Chem. Int. Ed.* **2007**, *46*, 3249–3251; *Angew. Chem.* **2007**, *119*, 3313; b) N. Leblanc, W. Bi, N. Mercier, P. Auban-Senzier, C. Pasquier, *Inorg. Chem.* **2010**, *49*, 5824–5833; c) N. Leblanc, M. Allain, N. Mercier, L. Sanguinet, *Cryst. Growth Des.* **2011**, *11*, 2064–2069; d) X.-Y. Lv, M.-S. Wang, Y. Chen, G.-E. Wang, S.-H. Wang, R.-G. Lin, G.-C. Guo, *Inorg. Chem.* **2012**, *51*, 4015–4017; e) R.-G. Lin, G. Xu, G. Lu, M.-S. Wang, P.-X. Li, G.-C. Guo, *Inorg. Chem.* **2014**, *53*, 5538–5545.
[7] Q.-X. Yao, Z.-F. Ju, X.-H. Jin, J. Zhang, *Inorg. Chem.* **2009**, *48*, 1266–1268.
[8] a) J.-K. Sun, P. Wang, Q.-X. Yao, Y.-J. Chen, Z.-H. Li, Y.-F. Zhang, L.-M. Wu, J. Zhang, *J. Mater. Chem.* **2012**, *22*, 12212–12219; b) J.-K. Sun, X.-H. Jin, L.-X. Cai, J. Zhang, *J. Mater. Chem.* **2011**, *21*, 17667–17672; c) X.-H. Jin, J.-K. Sun, X.-M. Xu, Z.-H. Li, J. Zhang, *Chem. Commun.* **2010**, *46*, 4695–4697; d) J.-K. Sun, P. Wang, C. Chen, X.-J. Zhou, L.-M. Wu, Y.-F. Zhang, J. Zhang, *Dalton Trans.* **2012**, *41*, 13441–13446.
[9] a) Y. Tan, H. Chen, J. Zhang, S. Liao, J. Dai, Z. Fu, *CrystEngComm* **2012**, *14*, 5137–5139; b) K. Fu, C. Chen, L.-X. Cai, B. Tan, J. Zhang, *CrystEngComm* **2014**, *16*, 5134–5141.
[10] a) Y. Zeng, Z. Fu, H. Chen, C. Liu, S. Liao, J. Dai, *Chem. Commun.* **2012**, *48*, 8114–8116; b) M.-S. Wang, C. Yang, G.-E. Wang, G. Xu, X.-Y. Lv, Z.-N. Xu, R.-G. Lin, L.-Z. Cai, G.-C. Guo, *Angew. Chem. Int. Ed.* **2012**, *51*; *Angew. Chem.* **2012**, *51*, 3432–3435.

[11] a) X.-H. Jin, C.-X. Ren, J.-K. Sun, X.-J. Zhou, L.-X. Cai, J. Zhang, *Chem. Commun.* **2012**, *48*, 10422–10424; b) A. D. Phillips, Z. Fei, W. H. Ang, R. Scopelliti, P. J. Dyson, *Cryst. Growth Des.* **2009**, *9*, 1966–1978.
[12] H. Kamogawa, T. Suzuki, *J. Chem. Soc., Chem. Commun.* **1985**, 525–526.
[13] Q.-X. Yao, W.-M. Xuan, H. Zhang, C.-Y. Tu, J. Zhang, *Chem. Commun.* **2009**, 59–61.
[14] Y. Ishii, N. P. Wickramasinghe, S. Chimon, *J. Am. Chem. Soc.* **2003**, *125*, 3438–3439.
[15] G. Kervern, G. Pintacuda, Y. Zhang, E. Oldfield, C. Roukoss, E. Kuntz, E. Herdtweck, J.-M. Basset, S. Cadars, A. Lesage, C. Copret, L. Emsley, *J. Am. Chem. Soc.* **2006**, *128*, 13545–13552.
[16] S. K. Kumara Swamy, A. Karczmarska, M. Makowska-Janusik, A. Kassiba, J. Dittmer, *ChemPhysChem* **2013**, *14*, 1864–1870.
[17] D. Santa Maria, R. M. Claramunt, S. F. Vasilevsky, S. V. Klyatskaya, I. Alkorta, J. Elguero, *ARKIVOC* **2011**, *3*, 114–127.
[18] O. Toma, N. Mercier, M. Allain, A. A. Kassiba, J. P. Bellat, G. Weber, I. Bezverkhyy, *Inorg. Chem.* **2015**, *54*, 8923–8930.
[19] F. Rastrelli, A. Bagno, *Chem. Eur. J.* **2009**, *15*, 7990–8004.
[20] The compound has been synthesized according to the following work, see: R. R. Das, J.-M. Lee, C.-H. Noh, S.-J. Jeon, U. S. Pat. *Appl.* Publ. **2012**, US 20120176658 A1 20120712; see the Supporting Information for details.
[21] G. Scalmani, V. Barone, B. Mennucci, G. A. Petersson, H. Nakatsuji, M. Caricato, X. Li, H. P. Hratchian, A. F. Izmaylov, J. Bloino, G. Zheng, J. L. Sonnenberg, M. Hada, M. Ehara, K. Toyota, R. Fukuda, J. Hasegawa, M. Ishida, T. Nakajima, Y. Honda, O. Kitao, H. Nakai, T. Vreven, J. A. Montgomery, Jr., J. E. Peralta, F. Ogliaro, M. Bearpark, J. J. Heyd, E. Brothers, K. N. Kudin, V. N. Staroverov, R. Kobayashi, J. Normand, K. Raghavachari, A. Rendell, J. C. Burant, S. S. Iyengar, J. Tomasi, M. Cossi, N. Rega, J. M. Millam, M. Klene, J. E. Knox, J. B. Cross, V. Bakken, C. Adamo, J. Jaramillo, R. Gomperts, R. E. Stratmann, O. Yazyev, A. J. Austin, R. Cammi, C. Pomelli, J. W. Ochterski, R. L. Martin, K. Morokuma, V. G. Zakrzewski, G. A. Voth, P. Salvador, J. J. Dannenberg, S. Dapprich, A. D. Daniels, Ö. Farkas, J. B. Foresman, J. V. Ortiz, J. Cioslowski, D. J. Fox, *Gaussian 09*, revision A.01, Gaussian, Inc., Wallingford, CT, USA, **2004**.

Received: October 19, 2015
Published Online: January 29, 2016

